

Cracking in ceramic/metal/polymer trilayer systems

Hong Zhao,^{a)} Pedro Miranda,^{b)} and Brian R. Lawn

Materials Science and Engineering Laboratory, National Institute of Standards and Technology, Gaithersburg, Maryland 20899-8500

Xiaozhi Hu

Department of Mechanical and Materials Engineering, The University of Western Australia, Nedlands, WA 6907, Australia

(Received 1 November 2001; accepted 15 February 2002)

Fracture and deformation in model brittle-outerlayer/metal-core/polymer-substrate trilayer systems in concentrated loading are studied. Model systems for experimental study are fabricated from glass microscope slides glued with epoxy adhesive onto steel and aluminum sheets, and the resulting laminates glued onto polycarbonate substrate bases. Critical loads to initiate two basic fracture modes in the glass layers—cone cracks at the top surfaces and radial cracks at the undersurfaces—are measured as a function of metal thickness by *in situ* observation through the glass side walls. Finite element modeling (FEM) is used to quantify these competing fracture modes. The more damaging radial fracture mode is attributed to flexure of the glass layers on soft underlayers. Although much of this flexure can be eliminated by removing the soft adhesive interlayer between glass and metal, yield in the metal limits the potential increases in critical load for radial cracking. Trilayer systems consisting of porcelain fused to Co-, Pd- and Au-alloy core support layers relevant to dental crowns are then analyzed by FEM. The hardness (especially) and elastic modulus of the metal are identified as the primary controlling material parameters, with modulus and strength of the brittle layer as supplemental parameters. Guidelines for improving metal-based crownlike layer structures are thereby developed via optimization of metal properties and relative layer thicknesses.

I. INTRODUCTION

Ceramic/metal/polymer layer structures are of interest in a wide range of biomechanical and other engineering applications. An illustrative example is found in traditional dentistry, where a porcelain ceramic veneer is fused to a stiff metal core to form an integral crown, which is then cemented onto a compliant dentin tooth base.¹ As with natural tooth enamel, the crown “shields” the compliant polymer-based dentin underlayer from external applied loads arising from contacts with opposing dentition. In such crown structures, the intended benefits of each component layer must be weighed against countervailing disadvantages. The outer porcelain veneer is hard and therefore provides wear resistance (as well as aesthetics); the metal core is stiff and tough, and so provides support without danger of itself fracturing. However, porcelain is relatively brittle and thus subject

to cone cracking at the top surface,² while metals are relatively soft and thus subject to yield below the oral contacts. Studies of bilayers made from thin porcelain plates fused to thick metal substrates have demonstrated how yield in the metal allows the overlaying brittle layer to flex, building up tensile stresses in the ceramic undersurface and thereby generating additional, comparatively dangerous subsurface radial cracks.^{3,4} Reducing the thickness of the metal support layer and placing the remnant bilayer plate onto a compliant polymer, in simulation of the crown/dentin trilayer structure, only enhances flexure of the top veneer layer, exacerbating the prospect of such radial cracking. Considerations of this kind are also relevant to the design of total hip replacements,^{5,6} specifically in the acetabular cups where various ceramic/metal/bone layered combinations have been proposed.

Accordingly, there is a need to study the fracture and deformation processes that characterize generic ceramic/metal/polymer layer structures. What are the best metals and the most effective layer thicknesses to minimize these damage processes? Why is it that in practice metal-based dental crowns have superior lifetimes relative to

^{a)}Present address: Vitreous State Laboratory, Catholic University of America, Washington, District of Columbia 20064.

^{b)}Visiting Professor, from Departamento Electrónica e Ingeniería Electromecánica, Escuela de Ingenierías Industriales, Universidad de Extremadura, 06071 Badajoz, Spain.

all-ceramic crowns with hard ceramic cores, even though the latter are stiffer and would therefore appear to offer greater support?^{1,7} A fundamental understanding of the implicit materials issues underlying such questions would appear to hold the key to improved lifetime performance of biomechanical structures.

In the present study, we examine cracking in model flat-layer glass/metal/polycarbonate trilayer systems. These structures are simple elaborations of previously studied ceramic/polymer^{8,9} and ceramic/metal bilayers.^{3,4} They are easily fabricated by bonding adjacent layers together with epoxy adhesive. Steel and aluminum are chosen for the metal core layers because of their ready availability and their disparate modulus and hardness properties; glass is chosen for its amenability to *in situ* observation of subsurface radial cracks; polycarbonate is an ideal compliant polymer substrate base material, with minimal viscoelastic complication. The trilayers are loaded at their top surfaces with a spherical indenter. Critical loads to produce subsurface radial cracks, as well as top-surface cone cracks, are measured as a function of metal layer thickness (glass thickness fixed) for each trilayer system. Finite element modelling (FEM) is used to evaluate the stresses responsible for the fracture and any underlying yield processes, and to confirm basic trends in the critical load data.

With the computational methodology validated for the model systems, FEM is then used to predict critical loads for lifetime-threatening damage in clinically relevant dental trilayer systems, specifically for porcelain veneers fused to Co-, Pd- and Au-alloy core layers *without* soft adhesive, on dentin substrates. Whereas critical loads for radial cracking in the veneer are the primary concern, it is argued that yield in the core is an important precursor factor in the failure mechanics, and that such yield may even lead to system failure of its own accord under extreme conditions. Guidelines for improving metal-based crownlike layer structures are thereby developed via optimization of metal properties and relative layer thicknesses to minimize potential failures.

II. EXPERIMENTAL AND ANALYTICAL PROCEDURE

A. Experiments on model trilayers

Model ceramic/metal/polymer trilayers for experimental testing were prepared in accordance with Fig. 1. Constituent layer materials, chosen in part for their ready availability, are shown in Table I, along with pertinent properties. Soda-lime glass microscope slides (Fischer Scientific, Pittsburgh, PA) of thickness $d_c = 1.2$ mm and surface dimensions 75×25 mm were used for the outer brittle ceramic layers. The utility of transparent glass as a model outerlayer material has been well documented

in analogous bilayer studies.^{8,9} As in those earlier studies, either top or bottom surfaces of the slides were pre-abraded with 600 SiC grit to reduce the scatter of data in the ensuing contact loading tests and to provide a means for independent examination of cone and radial crack systems. Common stock 416 stainless steel and aluminum sheets, ground to thicknesses in the range $d_m = 0.1$ to 4 mm and cut to the same lateral dimensions as the glass, were chosen for the core metal layers. These two metals embrace a broad range of modulus and hardness values. Polycarbonate slabs 12.5 mm thick (Hyzod, AIN Plastics, Norfolk, VA) were used as the polymer base layers. As with the glass, the utility of polycarbonate as a model compliant substrate has been well documented.^{8,9}

Basic materials characterization was carried out for each of the above constituent materials. Young's modulus E was measured by an ultrasonic method (Grindosonic MK5, J.W. Lemmens Inc., St. Louis, MO) and indentation hardness H was determined from Vickers indentations (Zwick 3212 Hardness tester, Zwick of America, East Windsor, CT). Indentation stress-strain curves were obtained using WC sphere indenters $r = 1.98$ to 12.7 mm, from measurements of contact radii a at specified loads P , yielding indentation stress $p_0 = P/\pi a^2$ as a function of indentation strain a/r .^{3,10} Strengths σ_F of abraded glass slides were measured in conventional four-point bending.⁸

The constituents in each trilayer structure were bonded together by epoxy adhesive (Harcos Chemicals, Bellesville, NJ), which was allowed to set under clamping

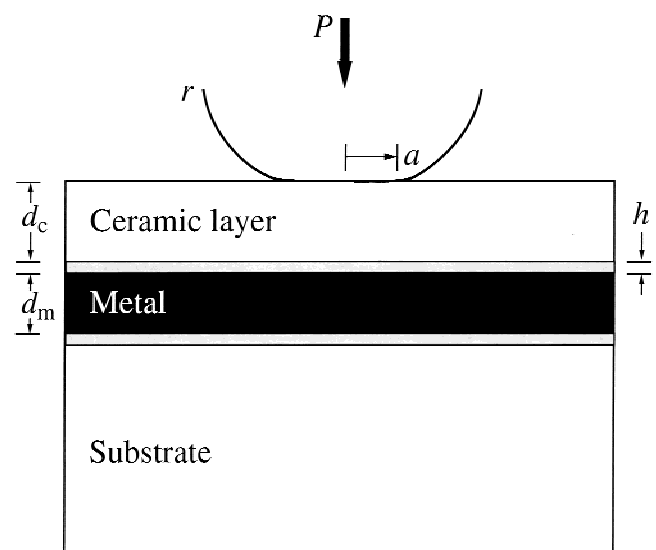


FIG. 1. Schematic diagram of a model flat ceramic/metal/polymer trilayer test configuration, ceramic outerlayer thickness d_c , and metal support core thickness d_m . Model specimens were bonded with epoxy adhesive with thickness h . The specimen is loaded in indentation with a WC sphere of radius r at load P .

pressure for 24 h at room temperature. Both sides of each trilayer specimen were polished for through viewing during ensuing contact testing. Interlayer adhesive thicknesses $h = 15 \pm 10 \mu\text{m}$ were measured by center-sectioning cured specimens after contact experimentation was complete.

Contact loading was applied to the top glass surfaces of the trilayer specimens with WC spheres of radius $r = 3.96 \text{ mm}$ at a fixed crosshead speed $0.2 \text{ mm}\cdot\text{min}^{-1}$ in air.⁸ The incidence of subsurface radial or top-surface cone cracking in the glass layers was observed *in situ* through the side walls during contact, with an optical zoom system (Optem, Santa Clara, CA) mounted into a video camcorder (Canon XL1, Canon, Lake Success, NY). Several indentation tests could be made on any one trilayer specimen surface.

Included in Table I are some materials used in the preparation of simulated metal-based crowns for later FEM analysis, with data taken from a previous study⁴: a veneering porcelain (Vita Omega 900, Vita Zahnfabrik, Bad Säckingen, Germany) and three core alloys—Co-alloy (Novarex, Jeneric/Pentron, Inc., Wallingford, CT), Pd-alloy (Argipal, Argen Precious Metals, San Diego, CA), and Au-alloy (Argident 88, Argen Precious Metals, San Diego, CA). Data for dentin are also shown.¹¹

B. Finite element modeling

A FEM algorithm was used to analyze the stresses in the model ceramic/metal/polycarbonate systems (complete with any adhesive interlayers), and to relate these stresses to the measured critical loads for radial cracking in the model trilayer systems. The procedure and grid detail have been detailed previously.¹² Basically, the algorithm models a deformable tungsten carbide

half-sphere indenter (radius $r = 3.96 \text{ mm}$) in frictionless axisymmetric contact with a well-bonded flat deformable multilayer (8 mm radius and 14 mm total thickness). The simulation is performed by first setting the sphere in contact with the flat specimen and then loading to a prescribed maximum value in 20 increments. For each layer, a bilinear constitutive elastic–plastic uniaxial stress–strain function $\sigma(\epsilon)$ is prescribed.^{13,14} Initially, each material deforms elastically, as defined by Young's modulus E and Poisson's ratio ν ; once yield occurs, the materials deform according to a linear strain hardening function of form $\sigma = Y + \alpha(\epsilon E - Y)$, with Y a uniaxial yield stress and α a dimensionless strain-hardening coefficient (values between 0, fully plastic, and 1, fully elastic).¹³

In the present study, Y and α were adjusted to fit indentation stress–strain data for each constituent material in Table I (glass, porcelain, and dentin assumed linear). Critical loads for fracture and yield were then evaluated for the composite trilayers, for specified layer thicknesses. Loads $P = P_R$ for radial cracking in the ceramic outer layers were determined by imposing the condition $\sigma_2 = \sigma_F$, with σ_2 the maximum principal out-of-plane hoop stress at the ceramic undersurface and σ_F the bulk ceramic strength (Table I). Similarly, loads $P = P_Y$ for yield in the metal layers were determined by imposing $\sigma_S = Y$, with $\sigma_S = \{1/2[(\sigma_1 - \sigma_2)^2 + (\sigma_2 - \sigma_3)^2 + (\sigma_3 - \sigma_1)^2]\}^{1/2}$ the von Mises stress.

FEM was also used to determine critical loads P_C for cone cracks. These cracks are governed by the in-plane σ_1 stresses in the near-contact region at the ceramic top surface, but in a complex manner, due to strong stress gradients along the crack path.¹⁵ To evaluate P_C we first calculate the peak value of σ_1 at the critical load for glass/metal bilayers, then determine the critical loads to attain this same peak stress level in the trilayers.⁴

TABLE I. Materials used in this study.

Material	Young's modulus ^a E (GPa)	Hardness ^b H (GPa)	Yield stress Y (GPa)	Strain-hardening coefficient α	Strength S (MPa)
Ceramics					
Glass	70	5.4	110
Porcelain	66	6.2	130
Metals					
Steel	199	1.8	0.40	0.006	...
Aluminum	71	0.77	0.20	0.005	...
Co-alloy	231	3.0	0.70	0.030	...
Pd-alloy	126	2.0	0.55	0.010	...
Au-alloy	92	1.2	0.37	0.001	...
Polymeric materials					
Polycarbonate	2.35	0.3	0.065	0.050	...
Epoxy adhesive	3.7	0.4	0.093	0.001	...
Dentin	18	1.0

^aPoisson's ratio $\nu = 0.22$ for veneer materials, $\nu = 0.35$ for metal cores and substrates.

^bHardness $H = \text{load}/\text{projected area of Vickers indentation} = 1.078H_V$.

III. RESULTS

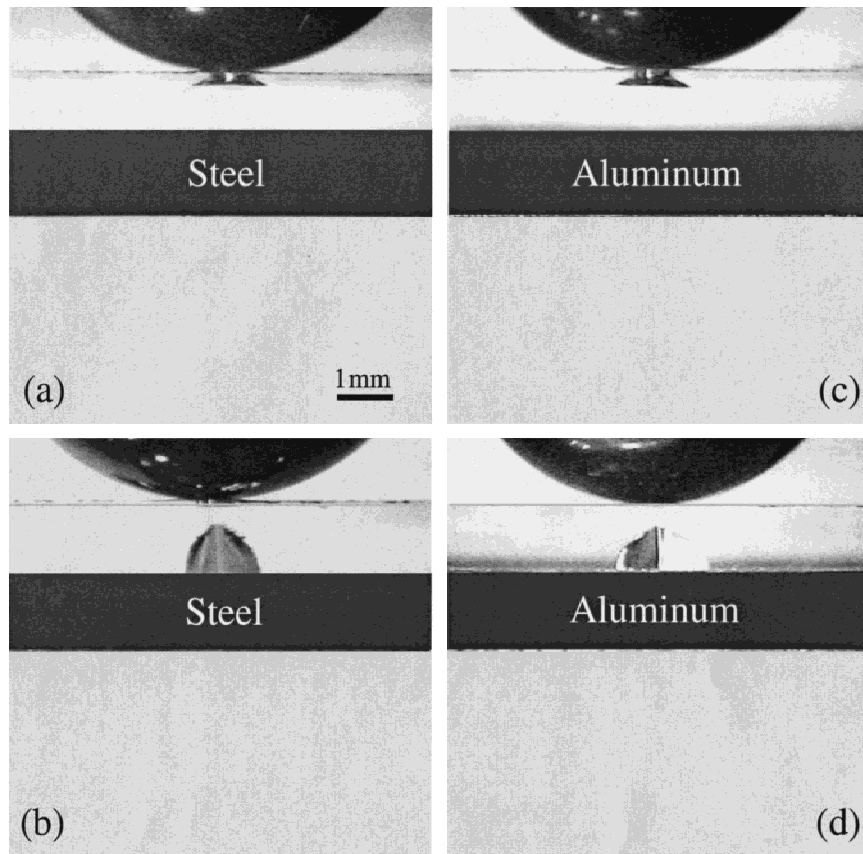
A. Data and analysis for adhesively bonded glass/metal/polycarbonate trilayers

Figure 2 shows micrographs of cone and radial cracks in glass overlayers (thickness $d_c = 1.2$ mm) on steel [Figs. 2(a) and 2(b)] and aluminum [Figs. 2(c) and 2(d)] core support layers (thickness $d_m \approx 1.5$ mm). For top-surface-abraded glass layers [Figs. 2(a) and 2(c)], ring cracks have initiated within the near-contact region into classical Hertzian cone configurations. For bottom-surface-abraded glass layers [Figs. 2(b) and 2(d)], radial cracks have initiated at the glass/metal interface into characteristic elongate pennylike configurations on median planes containing the contact axis (in the examples shown, the radials are inclined to the plane of the figure). In these examples both crack types remain wholly

contained within the glass layers at initiation, indicative of a structure with a degree of damage tolerance. On further increase of the applied loads, both crack types expanded; the radial cracks more rapidly, until ultimately one or other penetrated through the glass layer. At that point the glass/metal interfaces delaminated, leading to total failure of the trilayer.

Figure 3 plots measured critical loads for cracking in glass layers of fixed thickness ($d_c = 1.2$ mm) as a function of steel [Fig. 3(a)] or aluminum [Fig. 3(b)] core thickness d_m for model trilayers with adhesive interlayers. Data points are means and standard deviations (minimum 5 indentations): P_R for radial cracking (filled symbols, bottom-abraded glass surfaces), and P_C for cone cracking (unfilled symbols, top-abraded glass surfaces). Solid curves are FEM calculations of the functions $P_R(d_m)$ and $P_C(d_m)$, assuming a fixed adhesive thickness

Top glass surface abraded



Bottom glass surface abraded

FIG. 2. Optical side-view micrographs showing *in situ* crack initiation in glass/metal/polycarbonate trilayer of thicknesses $d_c = 1.2$ mm and $d_m \approx 1.5$ mm, on a thick (12.5 mm) polycarbonate substrate, during contact with a WC sphere, $r = 3.96$ mm. Steel core: (a) top glass surface abraded, showing a cone crack at $P = 525$ N; (b) bottom glass surface abraded, showing a radial crack at $P = 1210$ N. Aluminum core: (c) top glass surface abraded, cone crack at $P = 520$ N; (d) bottom glass surface abraded, radial crack at $P = 895$ N.

($h = 15 \mu\text{m}$) and using best-fit Y and α parameters (Table I) from the indentation stress-strain data for constituent materials in Fig. 4. (The P_C predictions are “truncated” at small d_m , where the fracture shifts from near-contact cone cracking to far-contact ring cracking.⁸) The FEM-generated curves confirm the basic data trends—i.e., increasing $P_R(d_m)$ and decreasing $P_C(d_m)$ —between limits at $d_m = 0$ for glass/polycarbonate bilayers⁸ and $d_m \rightarrow \infty$ for glass/metal bilayers.⁴ Once $d_m > d_c$, the $P_R(d_m)$ and $P_C(d_m)$ data saturate, signaling a shift in load-bearing capacity from the polycarbonate base to the intervening metal core layer. Some deviations between individual P_R data points and FEM curves in Fig. 3 may be attributed to scatter in actual values of h .¹²

Comparing metal cores, we see that $P_R(\text{steel}) > P_R(\text{aluminum})$ for any given d_m , affirming that the harder and stiffer metal provides better support against radial cracking, at least for the glass thickness and sphere radius used here. On the other hand, $P_C(\text{steel}) \approx P_C(\text{aluminum})$

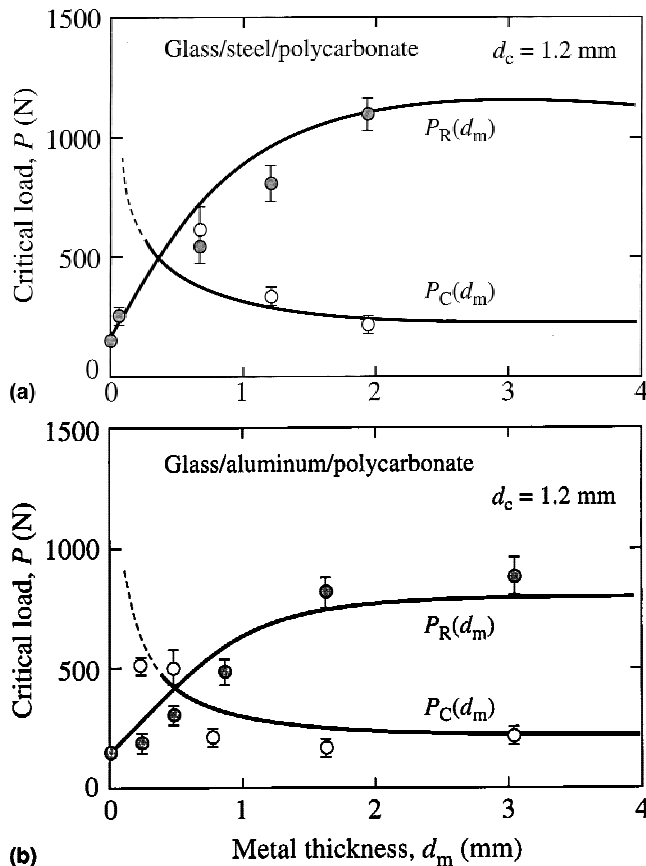


FIG. 3. Critical loads P_R and P_C for cracking in glass layer in model flat trilayers as function of metal support thickness d_m , at fixed $d_c = 1.2$ mm and WC sphere $r = 3.96$ mm: (a) glass/steel/polycarbonate and (b) glass/aluminum/polycarbonate. Experimental data (means and standard deviations) for trilayers with epoxy adhesive interlayers ($h = 15 \pm 10 \mu\text{m}$), showing data for radial cracking (filled symbols) and cone cracking (unfilled symbols). Solid lines are corresponding FEM calculations of $P_R(d_m)$ and $P_C(d_m)$ for fixed $h = 15 \mu\text{m}$.

over most of the d_m range, indicating that the metal support is not so important in surface cone cracking. Comparing the two crack types, $P_C < P_R$ for all $d_m \geq 0.6$ mm for both core metals, so that radial cracking would appear to be a secondary mode for trilayers with metal core thicknesses $d_m \geq 0.5d_c$.

B. FEM predictions for glass/metal/polycarbonate system with no adhesive

In many layer structures, e.g., porcelain/metal dental crowns, adjacent layers are fused together rather than joined by a soft adhesive. To illustrate the behavior of such structures, the validated FEM model is used to analyze glass/steel/polycarbonate and glass/aluminum/polycarbonate trilayers as above but with the adhesive interlayers removed. The residual interfaces are assumed to be infinitesimally thin ($h = 0$), to remain well bonded, and to have negligible residual stresses. Since even thin adhesive interlayers can facilitate flexure in overlying glass plates,⁹ such removal can be expected to result in substantial increases in the critical loads P_R for radial cracking¹²; in contrast, the critical loads P_C for cone cracking, governed largely by the near-contact Hertzian field, may be expected to be much less affected. Higher P_R translates to higher stress intensities in the metal cores, directing attention to prospective precursor yield in those layers.

Accordingly, Fig. 5 plots von Mises stress contours in two steel core layers, thicknesses $d_m = 1.5$ and 2.5 mm, for the same glass thickness ($d_c = 1.2$ mm) used in Fig. 3(a). The figure shows how shear stresses develop

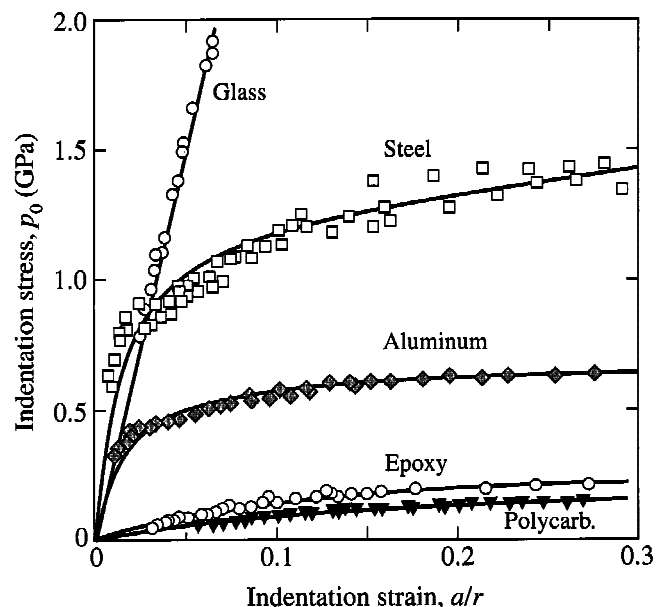


FIG. 4. Indentation stress-strain curves for constituent materials used in model trilayer experimental test specimens in this study. Curves are FEM fits using bilinear constitutive relation.

in the metal cores at loads up to and just beyond peak values for radial cracking, with black regions indicating yield zones. In the thinner steel layer [Fig. 5(a)–5(d)], yield occurs first at the bottom surface, at critical load $P_Y(\text{bottom})$; in the thicker layer [Fig. 5(e)–5(h)], yield occurs first at the top surface, at critical load $P_Y(\text{top})$. This inversion in first-yield location is consistent with a dominant core flexural stress field in the thinner metal layer and a dominant Hertzian contact field in the thicker metal layer. In both cases, yield initiates at one surface at threshold load, then at the other surface at higher load. Ultimately at even higher loads the opposing yield zones merge to form a “plastic hinge.” [In trilayers with very thin metal layers (not shown) yield spreads from the bottom surface through the layer without ever initiating separately at the top surface.] In no case were the shear stresses in the trilayers sufficient to exceed the yield point of polycarbonate over the load ranges covered, attesting to the capacity of the overlayers to shield the much more compliant substrate.

Figure 6 plots FEM-generated functions $P_R(d_m)$ for adhesive-free trilayers with elastic glass overlayers ($d_c = 1.2$ mm) and $P_Y(d_m)$ for plastic steel [Fig. 6(a)] and aluminum [Fig. 6(b)] cores. Results from Fig. 3 for comparative trilayers *with* adhesive are included as the dashed curve; the effect of eliminating the adhesive on the values of P_R is manifest. Also manifest is a strong correlation between P_R and $P_Y(\text{top})$ for both metal core systems, with $P_R \approx 2P_Y(\text{top})$ over a wide range of d_m . The maxima in $P_Y(d_m)$ and $P_R(d_m)$ at $d_m \approx d_c$ again reflect a transition from flexure-dominated to Hertzian-dominated shear stress fields. On the other hand, P_R does not appear to correlate at all strongly with $P_Y(\text{bottom})$. These trends, taken together, indicate the effectiveness of metal top-surface yield in facilitating glass flexure adjacent to the radial crack initiation site, compensating in part for removal of the adhesive interlayer. By way of confirmation, FEM-generated $P_R(d_m)$ functions for systems containing the same metals, but with yield artificially suppressed (infinite hardness), show relatively

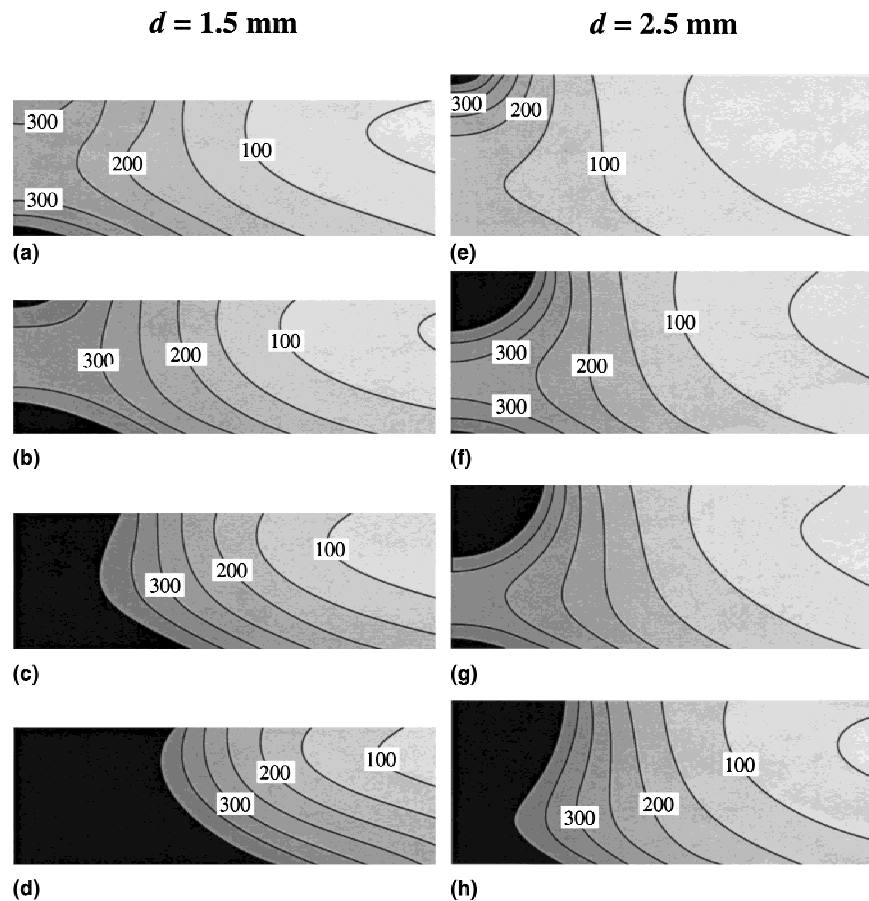


FIG. 5. FEM-generated contours of von Mises stresses in steel core layer for glass/steel/polycarbonate trilayers with no adhesive ($h = 0$) at increasing contact loads indicated (glass and polycarbonate layers not shown); WC sphere $r = 3.96$ mm. Plots for glass thickness $d_c = 1.2$ mm, and two steel thicknesses: $d_m = 1.5$, loads (a) $P = 1600$ N, (b) $P = 2000$ N, (c) $P = 2600$ N, (d) $P = 3400$ N; and $d_m = 2.5$ mm, loads (e) $P = 1800$ N, (f) $P = 3300$ N, (g) $P = 3600$ N, (h) $P = 4500$ N. Compare with Fig. 3(a). Each contour represents a stress increase of 50 MPa. Yield zones are indicated in black.

rapid and monotonic increasing critical loads, with virtually no prospect of radial cracking in trilayers with thicker cores.

It is clear from Fig. 6 that $P_{Y(top)}$ and P_R are consistently greater for trilayers with steel cores than with aluminum cores, confirming the advantage of stiffer and harder metals for both real and hypothetical systems with and without adhesive or metal yield.

IV. FEM SIMULATIONS FOR CROWN MATERIAL STRUCTURES

In this section we describe FEM calculations of critical contact loads to produce radial cracking P_R and yield P_Y in flat trilayers using more realistic dental crown materials (Table I): porcelain veneers fused onto Co-alloy,

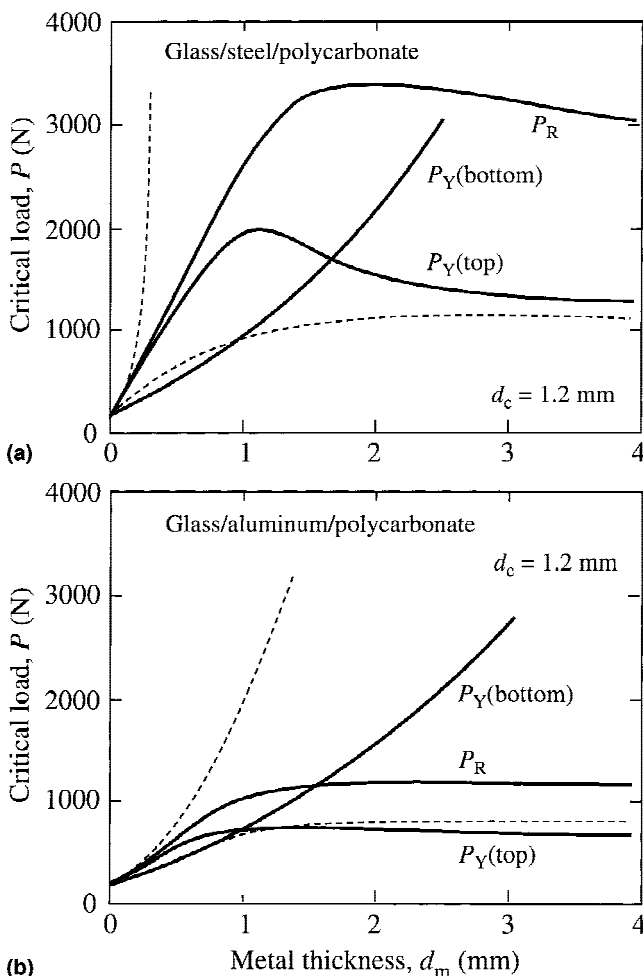


FIG. 6. FEM-computed critical loads for model flat trilayers without adhesive ($h = 0$; fixed glass thickness $d_c = 1.2$ mm; WC sphere $r = 3.96$ mm) as a function of d_m : (a) glass/steel/polycarbonate and (b) glass/aluminum/polycarbonate. Curves shown are $P_Y(d_m)$ for yield at the top and bottom metal surfaces and $P_R(d_m)$ for subsequent (post-yield) radial cracking. The lower dashed curve is calculated $P_R(d_m)$ for trilayer with intervening adhesive between glass and metal (from Fig. 3). The upper dashed curve is calculated $P_R(d_m)$ for hypothetical metal with no yield, and with no glass/metal interlayer adhesive.

Pd-alloy and Au-alloy cores,³ bonded to dentin substrates. Again, as in Sec. III. B, we assume no intervening adhesive at the porcelain/metal interface. However, in this case the net thickness of the porcelain/metal bilayer coating is held constant at $d = d_c + d_m = 1.5$ mm, relevant to physical limitations imposed on dental crowns. Input Y and α parameters (Table I) for the FEM computations are evaluated from fits to the indentation stress-strain data for the constituent materials shown in Fig. 7. The relative positions of the curves for the metals in Fig. 7 reflect the elastic modulus and hardness values in Table I. Porcelain, like glass, is elastic, and while dentin is surely deformable above a low yield stress ($Y \approx H/4 - H/3^{16}$), the “shielding” effect of the overlying “crown” layers prevents the dentin from entering the plastic domain.

FEM-generated functions $P_R(d_m)$ and $P_Y(d_m)$ for the trilayers are plotted for each of the metal alloy core layers in Fig. 8. Again, both $P_{Y(top)}$ and P_R show well-defined maxima, albeit more pronounced. These “sharper” maxima are attributable to the constraint of a fixed thickness d , so that as d_m increases d_c simultaneously diminishes, causing the porcelain/metal interface to migrate upward into the Hertzian contact field. This intensifies the shear stress in the metal top surface, resulting in a rapid falloff in $P_{Y(top)}$ and thereby also in P_R at large d_m . This latter Hertzian-dominated part of the curve will be dependent on the contacting sphere radius.

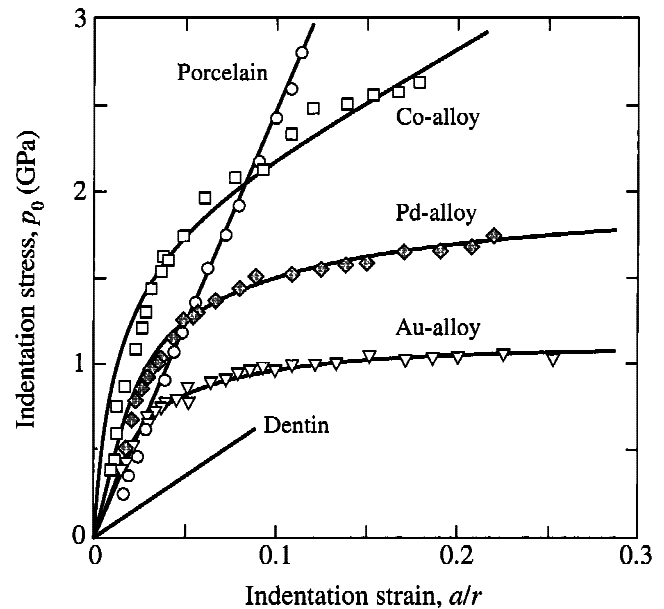


FIG. 7. Indentation stress-strain curves for constituent materials used in alternative trilayers consisting of dental materials: porcelain, Co-, Pd-, Au-alloys, dentin (elastic only). Curves are FEM fits using bilinear constitutive relation.

Once more, the relative values of $P_Y(\text{top})$ and P_R scale in some way with the modulus and hardness values of the metal alloy (Table I). However, the same is not true of $P_Y(\text{bottom})$, as we discuss below.

V. DISCUSSION

We have studied model trilayer structures consisting of brittle glass outer layers on stiff and tough metal support layers on elastically compliant polycarbonate

substrates, bonded together with thin, soft epoxy adhesive interlayers. Glass is used because of its transparency and well-documented fracture properties, plus its amenability to control of strength by surface abrasion (e.g., to match the strength of typical porcelains in dental crown simulations). In these structures, the primary mode of failure is radial cracking at the brittle layer undersurfaces; cone cracking in the near-contact regions at the top surfaces is a competing mode. Selective experiments on the model systems were used to validate an FEM algorithm simulating the contact process. With this validation, FEM predictions were made for specific metal-based trilayer systems pertinent to materials used in dental crowns. We showed that typical support core metals, although themselves generally immune to fracture, are susceptible to yield above some critical contact load P_Y , facilitating flexure of the overlying brittle layers and thence initiation of radial cracks at some higher load P_R . Consequently, the plastic as well as elastic properties of the metal core materials emerge as limiting factors in the design of metal-based layer structures.

A comparison between radial and cone crack data in Fig. 3 warrants further comment. It is seen that cone cracks occur at lower critical loads ($P_C < P_R$) over the bulk of the range of metal layer thickness (at $d_m \geq 0.6$ mm in Fig. 3). The rise in P_C at $d_m \leq 0.6$ mm is attributable to increasing compression in the top surface of the flexing glass plate on a thinner metal support. Since this rise correlates with a decline in P_R data in this region, we may take it as an indicator of increased tendency toward radial cracking in the bottom layer.⁴ This conclusion may be used to draw inferences on undersurface fracture tendencies in opaque coating materials. Of course, it is always wise to supplement any such inferences with specimen sectioning or other diagnostic techniques.^{3,4} Whereas radial cracking is relatively insensitive to contact conditions, cone cracking depends on sphere radius r in accordance with $P_C \propto r$ (Auerbach's law), and so will initiate at higher critical loads with blunter contacts,^{17,18} meaning that the value of d_m at the crossover between $P_C(d_m)$ and $P_R(d_m)$ curves will move further to the right as r increases. In any case, cone cracks are less likely than radial cracks to cause the system to fail and are thus of somewhat secondary interest in this kind of layer system.⁸

Figure 6 demonstrates that the removal of adhesive interlayers between top ceramic and support metal layers can greatly enhance P_R .^{9,12} Accordingly, care should be taken to keep any such adhesive interlayers as thin as possible or, preferably, to avoid them altogether. One way to accomplish the latter is to fuse the ceramic to the metal, as is done in the manufacture of porcelain-fused-to-metal dental crowns. Fused interfaces, on other hand, bring countervailing effects into play, e.g., residual stresses from thermal expansion mismatch. Such stresses

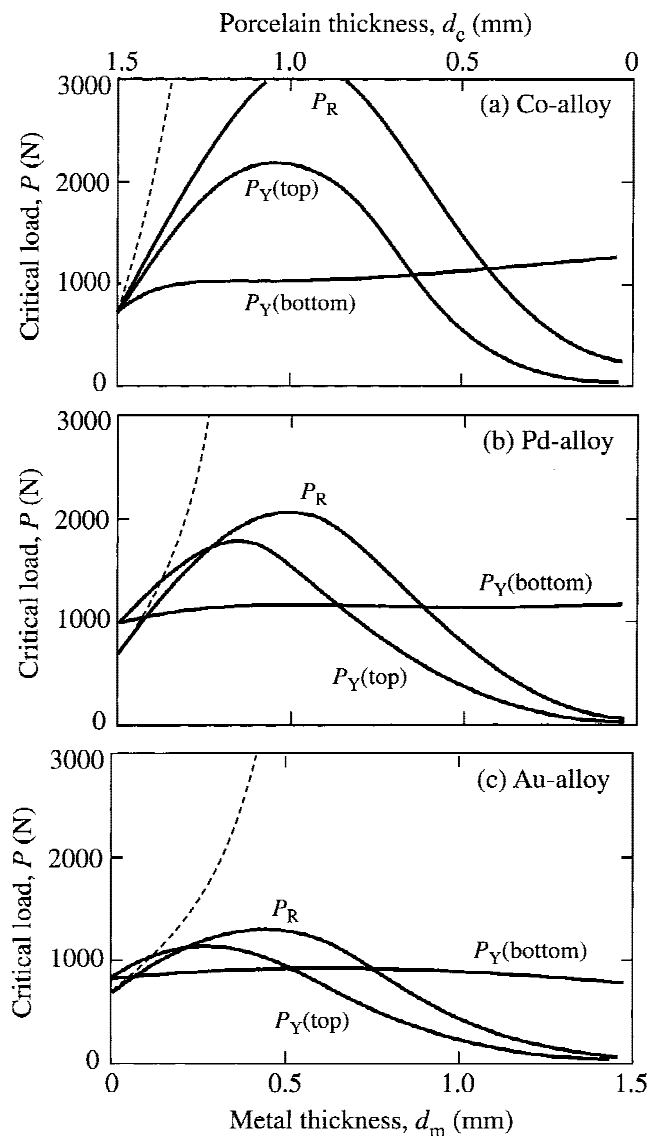


FIG. 8. FEM calculations of critical loads in flat crownlike porcelain/metal/dentin trilayers as function of metal thickness d_m , for fixed $d = d_c + d_m = 1.5$ mm, WC sphere $r = 3.96$ mm: (a) porcelain/Co-alloy/dentin, (b) porcelain/Pd-alloy/dentin, and (c) porcelain/Au-alloy/dentin. Plots are $P_Y(d_m)$ to produce yield (top and bottom surfaces) and $P_R(d_m)$ to produce radial cracking (including dashed curve for hypothetical metal with no yield).

can cause complications in fabrication (specifically from delamination) and, where tensile, can greatly enhance fracture in the brittle layer.

It is instructive to compare the current porcelain/metal/dentin trilayer computations with analogous porcelain/metal bilayer results from earlier studies.^{3,4} In the bilayers, yield begins at the top surface of the metal half-space at a critical load $P_Y = GH_m d_c^2$, $G = \alpha + \beta E_c/E_m$, with dimensionless coefficients $\alpha = 0.56$ and $\beta = 0.17$.⁴ Observe the linear dependence on the metal hardness and comparatively slow modulus-mismatch dependence. As intimated in Sec. I, we may think of the trilayer as a special case of the bilayer in which that portion of the metal substrate beyond depth $d = d_c + d_m$ (Fig. 1) is replaced by tooth dentin. To examine the effect of such a replacement we replot in Fig. 9 the $P_Y(d_m)$ results for first yield in Fig. 8 as $P_Y(d_c)$, in accordance with the constraining relation $d = d_c + d_m = 1.5$ mm, for each of the metal alloys (solid curves). These results may be compared with the corresponding $P_Y(d_c) = GH_m d_c^2$ predictions for porcelain metal bilayers, using the hardness and modulus values in Table I (dashed curves). Initially, both the trilayer and the bilayer P_Y curves increase monotonically with d_c , consistent with dominant yield in the metal top surfaces. In this region the hardness H_m remains the dominant material parameter; note how the position of the curves along the P_Y axis scales with the hardness values in Table I. The slightly higher trilayer curves relative to their bilayer

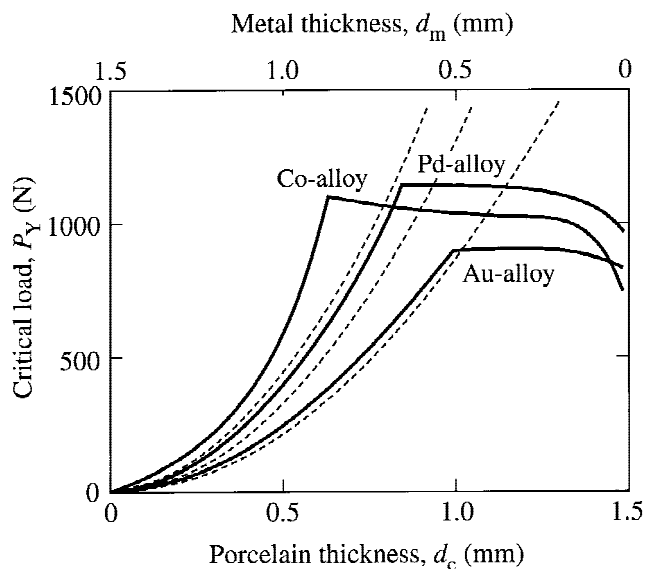


FIG. 9. Critical loads for first yield in different core metals in porcelain/metal/dentin trilayers as a function of porcelain thickness d_c for three metal alloy core materials, WC sphere $r = 3.96$ mm. The replot of curves from Fig. 8 is in accordance with constrained net crown thickness $d = d_c + d_m = 1.5$ mm. Solid curves are trilayers: the left segment of the curve corresponds to the top-surface yield in metal layer; the right segment corresponds to the bottom-surface yield. Dashed curves are bilayer equivalents (top-surface yield).

counterparts imply some diminution of the shear component of the Hertzian contact field associated with the compliant substrate. Above some transition porcelain thickness $d_c \approx d_m$, depending on the metal, the location of first yield switches from the top to the bottom metal surface, and the curves abruptly flatten out. The shear stresses in the metal layers are now dominated by flexure on the compliant dentin. In this region the curves no longer scale in the order of hardness values H_m , nor of elastic modulus E_m , indicating a more complex interplay between plastic and elastic properties.

The results above, particularly plots such as Fig. 9, serve as useful guidelines to the design of trilayers with metal support cores. The principal goal is simply to minimize radial cracking, i.e., keep $P < P_R$. (Cone cracking may be minimized by avoiding sharp contacts.) As demonstrated in Fig. 6, eliminating any soft adhesive interlayers between the brittle layer and metal is a first requirement, to restrict buildup of tensile stresses in the overlying brittle layer from contact-induced flexure. With this condition met, a high metal stiffness E_m is desirable, both to restrict flexure and to shield the compliant substrate from the external contact loads. It would also seem prudent to increase the strength σ_F of the brittle overlayer. However, as is evident from the computations for hypothetical elastic-brittle materials (Fig. 6), it is neither the elastic nor strength properties of the brittle layer that limit the trilayer response, but rather the yield properties of the metal core. Plasticity in the metal support greatly diminishes P_R by enhancing flexure in the brittle layer; in such cases, metal yield strongly enhances brittle fracture. Moreover, in extreme cases yield may lead directly to premature failure of the structure by delamination at the brittle-layer/metal-support interface, e.g., as a result of plastic deformation accumulation in fatigue loading.¹⁹ Accordingly, a more stringent and conservative design requirement is to ensure $P < P_Y$. Thus in Fig. 9 the goal is to remain beneath the $P_Y(d_c)$ curves. The first and obvious requirement is to keep the metal hardness H_m sufficiently high. Another requirement is to avoid the region of easy top-surface yield at left of the diagram. This means keeping the outer brittle layer sufficiently thick, i.e. $d_c \geq d_m$, but not so thick that the metal layer becomes too thin to protect the compliant substrate or to support the brittle overlayer. An added advantage of working in the region $d_c \geq d_m$ is that flexural compressive stresses in the top surface of the brittle layer will inhibit cone cracking, as indicated above.

Specific mention may be made of these requirements in the context of dental crown design. For the porcelain veneers, it is recommended that the thickness $d_c > 0.5$ mm at minimum, with even larger thickness for softer metal core support layers (Fig. 9). Strength, while not a limiting factor, should be maximized, particularly by

avoiding excessively large flaws. (Voids at the porcelain/metal interface could be most deleterious, by facilitating spurious flexure on the metal core.) For the metals, high hardness H_m is a primary requirement. The advantage of a high modulus E_m is less apparent: on the one hand, high E_m will help to shield the substrate and impede further radial cracking in the top layer; on the other, it will increase the flexure of the metal layer on the compliant substrate, promoting yield at the bottom surface in the recommended working region $d_c \geq d_m$. The curvature of crown surfaces should be maximized to restrict cone cracking. FEM analysis is currently the most convenient adjunct for quantifying these requirements for specific trilayer systems.

Finally, we return to a question posed in Sec. I: why do metal-based dental crowns have superior lifetimes relative to all-ceramic crowns with hard ceramic cores?^{1,7} We have demonstrated that the performance of metal-core structures is limited by yield, which can promote fracture in the veneer. Replacement of the metal with a ceramic of relatively high stiffness and, especially, high hardness, would appear to offer potentially greater protection of the veneer, as well as of the substrate. However, even the toughest ceramics remain brittle, and so are themselves highly susceptible to radial cracking from high tensile stresses at the flexing undersurfaces.¹² Moreover, the stiffer the ceramic core layer, the more the stress is transferred to that layer. In that case it is the strength rather than hardness of the core material that becomes the limiting factor. The relative virtues of such systems need to be explored further.

ACKNOWLEDGMENTS

This study was supported in part by National Institute of Standards and Technology (NIST) internal funds, the Junta de Extremadura–Consejería de Educación, Ciencia

y Tecnología y el Fondo Social Europeo, Spain (Grant Nos. BRV010007 and IPR00A084), and by the United States National Institute of Dental Research. Information on product names and suppliers in this paper does not imply endorsement by NIST

REFERENCES

1. J.R. Kelly, *J. Prosthet. Dent.* **81**, 652 (1999).
2. I.M. Peterson, A. Pajares, B.R. Lawn, V.P. Thompson, and E.D. Rekow, *J. Dent. Res.* **77**, 589 (1998).
3. H. Zhao, X.Z. Hu, M.B. Bush, and B.R. Lawn, *J. Mater. Res.* **15**, 676 (2000).
4. H. Zhao, X. Hu, M.B. Bush, and B.R. Lawn, *J. Mater. Res.* **16**, 1471 (2001).
5. A.W. Eberhardt, J.L. Lewis, and L.M. Keer, *ASME J. Biomed. Eng.* **113**, 410 (1991).
6. G. Willmann, *Adv. Eng. Mech.* **3**, 135 (2001).
7. J.R. Kelly, *Ann. Rev. Mater. Sci.* **27**, 443 (1997).
8. H. Chai, B.R. Lawn, and S. Wuttiphpan, *J. Mater. Res.* **14**, 3805 (1999).
9. H. Chai and B.R. Lawn, *J. Mater. Res.* **15**, 1017 (2000).
10. H. Cai, M.A. Stevens Kalceff, and B.R. Lawn, *J. Mater. Res.* **9**, 762 (1994).
11. H.H.K. Xu, D.T. Smith, S. Jahanmir, E. Romberg, J.R. Kelley, and V.P. Thompson, *J. Dent. Res.* **77**, 472 (1998).
12. P. Miranda, A. Pajares, F. Guiberteau, F.L. Cumbreira, and B.R. Lawn, *J. Mater. Res.* **16**, 115 (2001).
13. A.C. Fischer-Cripps and B.R. Lawn, *J. Am. Ceram. Soc.* **79**, 2609 (1996).
14. A.C. Fischer-Cripps, B.R. Lawn, A. Pajares, and L. Wei, *J. Am. Ceram. Soc.* **79**, 2619 (1996).
15. B.R. Lawn, *J. Am. Ceram. Soc.* **81**, 1977 (1998).
16. D. Tabor, *Hardness of Metals* (Clarendon, Oxford, United Kingdom, 1951).
17. Y-W. Rhee, H-W. Kim, Y. Deng, and B.R. Lawn, *J. Am. Ceram. Soc.* **84**, 561 (2001).
18. Y-W. Rhee, H-W. Kim, Y. Deng, and B.R. Lawn, *J. Am. Ceram. Soc.* **84**, 1066 (2001).
19. S. Suresh, *Fatigue of Materials* (Cambridge University Press, Cambridge, United Kingdom, 1991).